Phosphorylation of Tau protein correlates with changes in hippocampal theta oscillations and reduces hippocampal excitability in Alzheimer's model

Received for publication, November 29, 2017, and in revised form, March 14, 2018 Published, Papers in Press, April 9, 2018, DOI 10.1074/jbc.RA117.001187

Siddhartha Mondragón-Rodríguez[‡§1], Anahí Salas-Gallardo[§], Perla González-Pereyra[§], Martín Macías[§], Benito Ordaz[§], Fernando Peña-Ortega[§], Azucena Aguilar-Vázquez[§], Erika Orta-Salazar[§], Sofía Díaz-Cintra[§], George Perry[¶], and Sylvain Williams[‖]

From the [‡]CONACYT National Council for Science and Technology, 03940 México, México, [§]UNAM Developmental Neurobiology and Neurophysiology, Institute of Neurobiology, National Autonomous University of México, 76230 Querétaro, México, the [¶]UTSA Neuroscience Institute and Department of Biology, College of Sciences, University of Texas at San Antonio, San Antonio, Texas 78249, and the [‖]Department of Psychiatry, Douglas Mental Health University Institute, McGill University, Quebec H4H 1R3, Canada

Edited by Paul E. Fraser

Tau hyperphosphorylation at several sites, including those close to the microtubule domain region (MDr), is considered a key pathological event in the development of Alzheimer's disease (AD). Recent studies indicate that at the very early stage of this disease, increased phosphorylation in Tau's MDr domain correlates with reduced levels of neuronal excitability. Mechanistically, we show that pyramidal neurons and some parvalbumin-positive interneurons in 1-month-old triple-transgenic AD mice accumulate hyperphosphorylated Tau protein and that this accumulation correlates with changes in theta oscillations in hippocampal neurons. Pyramidal neurons from young triple-transgenic AD mice exhibited less spike accommodation and power increase in subthreshold membrane oscillations. Furthermore, triple-transgenic AD mice challenged with the potassium channel blocker 4-aminopyridine had reduced theta amplitude compared with 4-aminopyridine–treated control mice and, unlike these controls, displayed no seizure-like activity after this challenge. Collectively, our results provide new insights into AD pathogenesis and suggest that increases in Tau phosphorylation at the initial stages of the disease represent neuronal responses that compensate for brain circuit overexcitation.

Alzheimer's disease (AD)[2] is characterized by cognitive deficits that are correlated with aberrant hippocampal activity (1, 2). The hippocampus, which plays a critical role in learning and memory, is dramatically affected by the extracellular β-amyloid (Aβ) plaques and intracellular Tau neurofibrillary tangles mainly comprised of hyperphosphorylated Tau protein (3). Because of this neuropathological correlation, the two lesions have been proposed as the main culprit of AD (4–6). However, a new hypothesis that has emerged in recent years implicates brain activity alterations that lead to hippocampal memory loss and precede classical AD lesions (2, 7). The brain activity alterations would be enough to impair hippocampal synaptic plasticity, which translates into memory deficit (2, 8). Although the mechanism responsible for these early pathological changes remains elusive, soluble fragments of Aβ and hyperphosphorylated Tau protein have been suggested to trigger them (2, 9). For instance, impaired hippocampal activity can be induced by dendritic missorting of hyperphosphorylated Tau protein (9), whereas Aβ oligomers can induce Tau phosphorylation at pathological sites such as Ser^{199}, Thr^{217}, Thr^{231}, Ser^{235}, Ser^{396}, Ser^{404}, and Ser^{422} (10), which are located close to the microtubule domain region (MDr) of Tau protein (11). However, we have shown that Aβ-induced Tau phosphorylation at Tht^{231}, Ser^{235}, Ser^{396}, and Ser^{404} down-regulates *N*-methyl-D-aspartate (NMDA) receptor function, promoting the induction of long-term depression, a type of synaptic plasticity critical for learning (11). Our data suggest that phosphorylation of Tau MDr sites could modulate synaptic transmission, plasticity, and oscillatory activity, thus preventing Aβ-induced NMDA-mediated overexcitation (11, 12). Accordingly, increased Tau phosphorylation at pathological site Ser^{205} was found to decrease the susceptibility to Aβ excitotoxicity (13). Moreover, studies have reported very early accumulation of abnormally phosphorylated Tau at site Thr^{231} in the parvalbumin-positive (PARV+) hippocampal interneurons, which could contribute to changes in hippocampal activity (14).

Here, we used a young triple-transgenic AD (3xTg-AD) mouse model (1 month old) (15) and tested whether very early phosphorylation of Tau MDr sites could correlate with changes in hippocampal activity and lower predisposition to hyperexcitability. The 3xTg-AD mice harbor mutated human (amyloid precursor protein, APP), Tau, and PS1 genes and exhibit cog-

This work was supported CONACYT Grants 612271 and 770620 (to P. G.-P. and A. S.-G.), CONACYT Grants 269021 and 117-235789, DGAPA-UNAM Grant IN202018, fund from the Fundación Marcos Moshinsky, and National Institute of Minority Health and Health Disparities Grant G12MD007591 from the National Institutes of Health and by the Semmes Foundation. The authors declare that they have no conflicts of interest with the contents of this article. The content is solely the responsibility of the authors and does not necessarily represent the official views of the National Institutes of Health.

[1] Awarded a Cátedra position from the CONACYT. To whom correspondence should be addressed: Developmental Neurobiology and Neurophysiology, UNAM, Blvd. Juriquilla 3001, Juriquilla, 76230 Santiago de Querétaro, Qro, México. Tel.: 442-238-1057; E-mail: sidmonrod@gmail.com.

[2] The abbreviations used are: AD, Alzheimer's disease; MDr, microtubule domain region; 4-AP, 4-aminopyridine; Aβ, β-amyloid; NMDA, *N*-methyl-D-aspartate; PARV+, parvalbumin-positive; P*n*, postnatal day *n*; ACSF, artificial cerebrospinal fluid.

nitive impairments related to Aβ and Tau pathology as early as 4 months of age (15). To determine potential changes in the hippocampal circuit of the young 3xTg-AD model, we measured the level of excitability and oscillatory activity (proposed to be involved in memory storage and information processing (16)) by recording the intrinsic spontaneously generated CA1/subiculum theta oscillations.

Our data revealed that in the young 3xTg-AD model, Tau directly accumulates in pyramidal neurons and in some PARV+ hippocampal interneurons. Importantly, the hippocampus is known for generating theta activity because of coordinated synchronous activity of multiple neuronal assemblies, including PARV+ and pyramidal cells (17). Moreover, our findings showed that the detected changes in brain activity precede cognitive deficits. Finally, our data indicated that the increase in Tau phosphorylation at Tau MDr sites correlates with a lower predisposition to 4-aminopyridine (4-AP) overexcitation of the hippocampal circuitry.

Results

Tau phosphorylation increases in 3xTg-AD mice

To explore the possibility that MDr Tau phosphorylation increases at very early stages, we measured the levels of Tau phosphorylation in the young P30 mice (Fig. 1*A*). Western blotting analysis of total protein revealed an increase in phosphorylated Tau at the Ser^{396} site in the 3xTg-AD mice when compared with the family related non-Tg group (Fig. 1*B*). Statistical analysis further confirmed our findings, because a significant 3.18 $\pm$ 0.32-fold increase was found in the levels of phosphorylated Tau at the Ser^{396} site in the 3xTg-AD mice when compared with non-Tg mice (Fig. 1*C*). The presence of phosphorylated Tau protein in non-Tg mice was barely detected (data not shown). Notably, phosphorylated Tau protein was found coexisting along the entire pyramidal population in the young 3xTg-AD mice (Fig. 1*D*). The presence of phosphorylated Tau was clearly observed coexisting with the pyramidal cell layer of CA1 (Fig. 1*E*). Importantly, pyramidal neurons are responsible for generating synchronous neuronal activity including theta rhythms (18). Although the subiculum showed a lower number of pyramidal cells coexisting with Ser^{396}, no significant differences were detected when compared with the CA1 or CA3 regions (Fig. 1*F*, insert). Taken together, and consistent with our previous findings (3), our data showed that sites located at the Tau C-terminal domain increase at initial stages of disease progression. Thus, phosphorylated Tau preferentially coexists with the pyramidal cell layer of the entire hippocampus of the young 3xTg-AD mice model.

Tau phosphorylation increases in N terminus Tau sites

To further study Tau phosphorylation sites close to their MDr, we evaluated the levels of Tau phosphorylation at sites Thr^{231}–Ser^{235} labeled by mAb AT180 (Fig. 2*A*). In agreement with our previous data, the presence of phosphorylated Tau protein at sites Thr^{231} and Ser^{235} was found coexisting along the entire pyramidal population in the young P30 3xTg-AD mice (Fig. 2*A*). The increase of phosphorylation levels at sites Thr^{231}–Ser^{235} is clearly observed in the pyramidal cell from the hippocampus (Fig. 2*B*). The presence of phosphorylated N terminus Tau sites in non-Tg mice was barely detected (data not shown). Importantly, some PARV+ hippocampal interneurons in P30 3xTg-AD mice (Fig. 2*C*) accumulate phosphorylated forms of Tau (Fig. 2*D*, see merge in 2*E*). A more detailed analysis of AT180–positive PARV+ cells in P30 3xTg-AD mice (Fig. 2*F*) revealed a diffuse phospho-Tau positive staining within the cytoplasm, sometimes comprising small punctate regions (Fig. 2*G*, see merge in 2*H*). Surprisingly, entorhinal neurons express lower levels of phosphorylated Tau when compared with hippocampal pyramidal neurons (Fig. 2*I*).

Network oscillatory activity at theta band frequency is altered in young 3xTg-AD mice

The network oscillatory activity can be evaluated by performing extracellular recordings in the complete *in vitro* septohippocampal preparation (17, 20). We first studied the main properties of endogenous hippocampal oscillations in the middle CA1/subiculum area of the 3xTg-AD mice when compared with family-related non-Tg mice. Importantly, our recordings were performed at 30 days of postnatal age (P30) in all groups (see "Experimental procedures"). In line with our previous findings (21, 22), oscillatory activity from the non-Tg group showed rhythmic theta activity (3–8 Hz) in the CA1 and subiculum areas, characterized by stable power and frequency (Fig. 3*A*; see also magnification in Fig. 3*B*). Filtered traces at theta band frequency further confirmed the presence of rhythmic hippocampal theta activity (Fig. 3*C*). In contrast, hippocampal activity recorded from 3xTg-AD mice displayed altered theta rhythmicity (Fig. 3*D*; see also magnification in Fig. 3*E* and filtered traces in Fig. 3*F*). The spectrogram analysis showed a regular power band at theta frequency in the non-Tg mice (Fig. 3*G*). In contrast, the 3xTg-AD mice showed an irregular theta pick power band (Fig. 3*H*). Statistical analysis further confirmed rhythmic alterations in the middle CA1/subiculum area of 3xTg-AD mice (Fig. 3*I*). The average strength of theta oscillations recorded from the non-Tg group was significantly higher than that of the 3xTg-AD group (non-Tg: 0.034 $\pm$ 0.02 and 3xTg-AD: 0.002 $\pm$ 0.0004, Fig. 3*I*). Theta peak frequency analysis further confirmed an increase in the theta frequency band in 3xTg-AD mice when directly compared with non-Tg mice (Fig. 3*J*). The average frequency of theta oscillations from the non-Tg and 3xTg-AD groups was 2.76 $\pm$ 0.36 Hz and 4.51 $\pm$ 0.91 Hz, respectively (Fig. 3*J*). Statistical analysis also confirmed a significant increase in hippocampal theta frequency activity in the 3xTg-AD mice when compared with the non-Tg mice (Fig. 3*J*). To summarize, our study revealed rhythmic alterations at the theta frequency band in the CA1/subiculum of young 3xTg-AD mice when directly compared with family-related non-Tg mice (Fig. 3*K*).

To determine whether intrinsic properties of pyramidal cells are altered in 3xTg-AD mice, we performed patch–clamp recordings (Fig. 3*L*). Action potential properties were examined using current steps of increasing amplitude (see "Experimental procedures"). Although the amplitude and frequency of action potentials across different stimulus intensities did not differ between the 3xTg-AD and non-Tg groups, a significant power increase in subthreshold membrane oscillations was observed in the 3xTg-AD group (Fig. 3*M* and Table 1). In accordance,

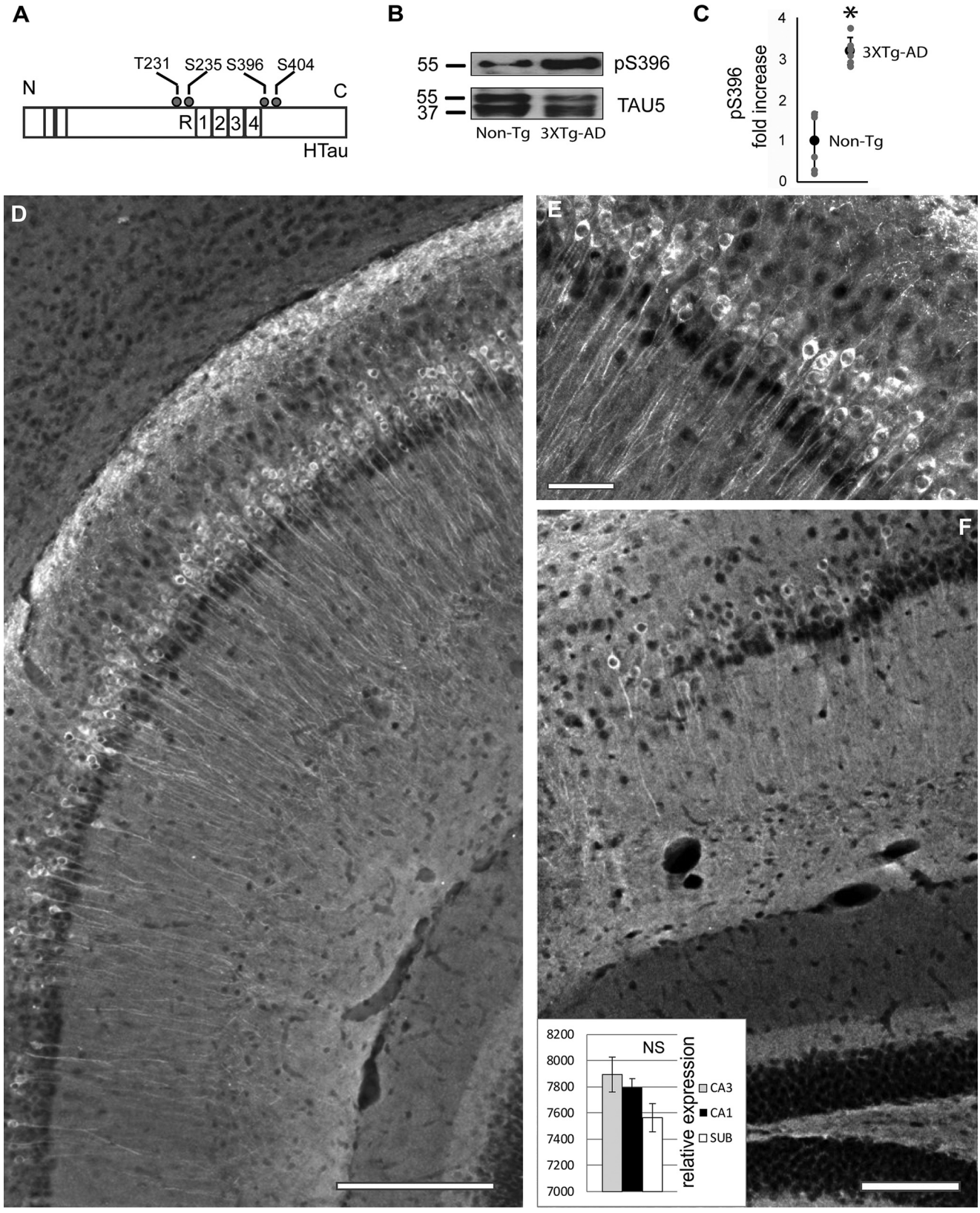

Figure 1. Tau phosphorylation was found increased in Tau C-terminal domain. *A*, Tau protein contains multiple phosphorylation sites such as Thr^{231}, Ser^{235}, Ser^{393}, and Ser^{404}. *B*, Tau phosphorylation levels increased at P30 in 3xTg-AD mice. No significant changes were identified in the levels of total Tau protein detected by mAb TAU5. *C*, the increase of Tau phosphorylation in the 3xTg-AD group at sites labeled by mAb Ser^{396} was statistically confirmed. *D*, phosphorylation of Tau protein at site Ser^{396} was found coexisting with the pyramidal neurons from the subiculum/CA1/CA2 region. *E*, Tau phosphorylation at Ser^{396} is clearly seen in the pyramidal cell layer of CA1. *F*, fewer cells were labeled in the subiculum area (*SUB*). No significant changes were detected between labeled areas (see *inset* in *F*), $n = 6$ in each group. All *bar graphs* show means ± S.E. *, $p < 0.05$; *NS*, $p \geq 0.05$. *Scale bars*, 200 (*D*), 50 (*E*), and 100 (*F*) μm.

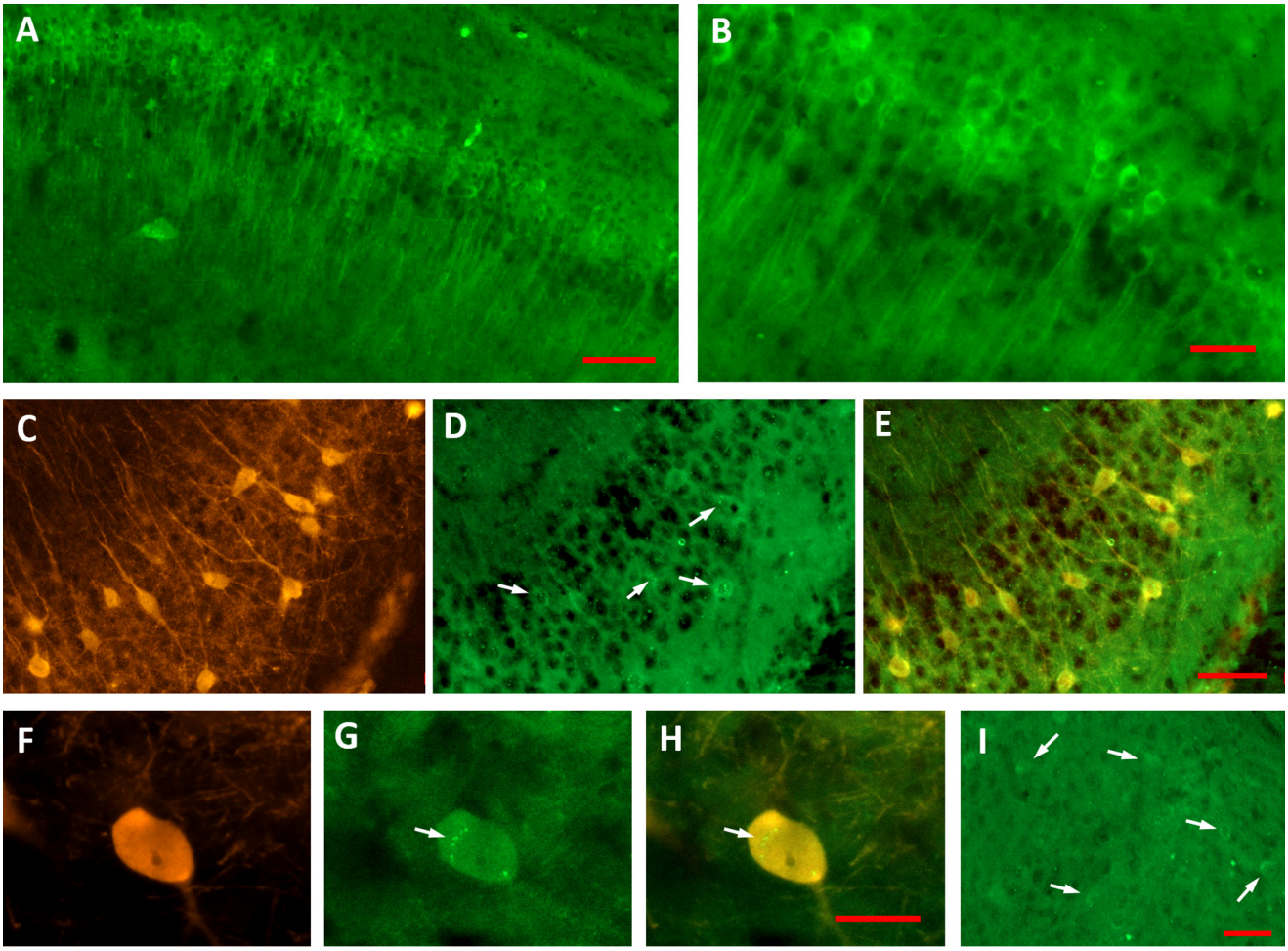

Figure 2. Tau phosphorylation was found increased in Tau N-terminal domains. *A* and *B*, the increase of Tau phosphorylation in 3xTg-AD group at sites labeled by mAb AT180 was found coexisting with the pyramidal neurons from the CA1/subiculum (*A*). A magnification is shown in *B*. *C–E*, PARV+ hippocampal interneurons (*C*) accumulate phosphorylated forms of Tau (*D* and *E*, *white arrows*). *F–H*, AT180–positive PARV+ interneurons (*F*) revealed punctate accumulation of phospho-Tau (*G* and *H*, *white arrows*). Entorhinal neurons displayed lower levels of phospho-Tau (*I*, *white arrows*). *Scale bar* for *A*, 100 μm; *scale bars* for *B–E*, 50 μm; *scale bar* for *F–H*, 20 μm; and *scale bar* for *I*, 50 μm.

pyramidal cells from 3xTg-AD mice showed less spike accommodation (non-Tg: 9.48 ± 1.93 and 3xTg-AD: 2.22 ± 0.45, Fig. 3*N* and Table 1).

Early brain circuit changes were independent of hippocampus-dependent behavioral task

To address the hippocampal function in our young 3xTg-AD group, we performed the burrowing and nesting tests (23, 24) (see "Experimental procedures"). Importantly, cytotoxic lesions in the hippocampus directly translate into significant reductions in the burrowing test (25). In contrast, medial prefrontal cortex lesions only induce a smaller reduction in the burrowing test (26). Thus, the burrowing test can be applied at early postnatal developmental ages (27). In the same vein, nesting is another assay that can be used to screen hippocampal-dependent behavioral alterations in young mice (24). In the burrowing test, the amount of displaced food pellets was measured after 2 and 12 h (Fig. 4*A* and 4*B*). The amount of food pellets removed from the burrow by animals belonging to the P30 3xTg-AD group was not significantly different from the number removed by animals belonging to the non-Tg group at either 2 h (Fig. 4*A*) or 12 h (Fig. 4*B*). To further evaluate hippocampal-dependent behavior of 3xTg-AD mice, we performed the nesting assay (Fig. 4*C*). Consistent with our burrowing findings, we did not find significant differences between non-Tg and 3xTg-AD mice in the nesting scores (Fig. 4*C*). In sum, the 3xTg-AD mice displayed no signs of hippocampal function deficits at the early postnatal developmental age of P30.

Hippocampal network hyperexcitability was reduced in the 3xTg-AD mice

We recently reported that hippocampal network excitability is increased in the TgCRND8 AD mice (22). This mice is characterized by Aβ deposition at 20 weeks of age (6). Interestingly, in contrast to non-Tg mice, blocking of Kv potassium channels with 4-AP in TgCRND8 at postnatal developmental stages (P30) increased theta power and induced seizure activity (22). To examine the network excitability of 3xTg-AD mice in the same experimental conditions, we bath-applied 4-AP while recording the complete septo-hippocampal preparation obtained from non-Tg and 3xTg-AD mice. Treatment with 4-AP elicited an increase in theta amplitude in the non-Tg group (Fig. 5*A*, *black rectangle*), which was followed by seizure-like activity (Fig. 5*A*, see magnification in the *lower panel*), characterized by

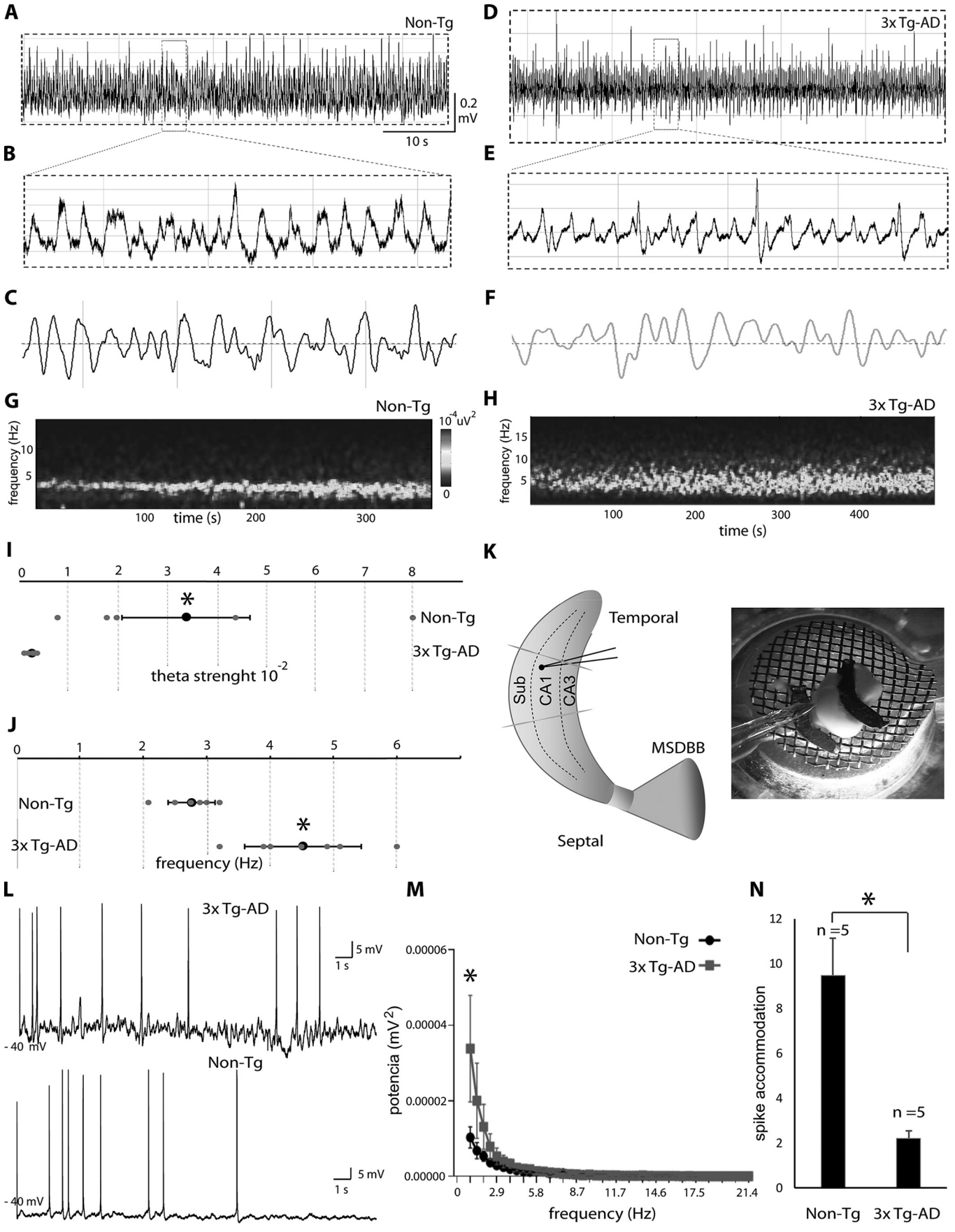
A
Non-Tg
0.2 mV
10 s
B
C
D
3x Tg-AD
E
F
G
Non-Tg
frequency (Hz)
10
5
10^{-4} uV^2
0
100
time (s)
200
300
H
3x Tg-AD
frequency (Hz)
15
10
5
100
200
300
400
time (s)
I
0 1 2 3 4 5 6 7 8
Non-Tg
3x Tg-AD
theta strenght 10^{-2}
J
0 1 2 3 4 5 6
Non-Tg
3x Tg-AD
frequency (Hz)
K
Temporal
Sub
CA1
CA3
MSDBB
Septal
L
3x Tg-AD
5 mV
1 s
- 40 mV
Non-Tg
5 mV
1 s
- 40 mV
M
Non-Tg
3x Tg-AD
potencia (mV^2)
0.00006
0.00004
0.00002
0.00000
0 2.9 5.8 8.7 11.7 14.6 17.5 21.4
frequency (Hz)
N
n =5
n =5
spike accommodation
12
10
8
6
4
2
0
Non-Tg
3x Tg-AD

Table 1

Membrane and firing properties of pyramidal cells in 3xTg-AD mice

All values are means ± S.E. ($n = 5$ for pyramidal cells from Non-Tg mice and $n = 5$ from 3xTg-AD mice). Independent t test comparisons produced significant differences for spike frequency adaptation and subthreshold membrane oscillations ($p < 0.05$). Maximal firing frequency was calculated from the total number of spikes elicited by 600-ms-long current injections of 200 pA above the firing threshold. Spike frequency adaptation was calculated as the normalized ratio of the instantaneous frequency at the first and last spike intervals in an action potential train (first − last/first). *, $p < 0.05$.

	Non-Tg	3xTg-AD
Resting potential (mV)	−62 ± 4.2	−65 ± 3.8
Membrane resistance (MΩ)	339.56 ± 45.99	350.77 ± 54
Subthreshold membrane oscillations ($mV^2 \times 10^{-4}$)	0.11 ± 0.039	0.15 ± 0.031*
Spike frequency adaptation	9.48 ± 1.93	2.22 ± 0.45*

ictal discharges (28). Conversely, 4-AP treatment in 3xTg-AD mice did not elicit a visible increase in theta amplitude (Fig. 5*B*). Contrary to the non-Tg group, 4-AP treatment caused a reduction in theta amplitude, and no seizure-like activity was observed (Fig. 5*B*). Further supporting our findings, zero Mg^{2+} did not elicit detectable changes in the amplitude and frequency of theta activity in the 3xTgAD mice (Fig. 5*C*).

Statistical analysis further confirmed our findings, because a significant increase in theta magnitude was found during and after 4-AP stimulation in the non-Tg group (3.53 ± 0.90-fold increase when compared with baseline) (Fig. 5*D*). No significant changes were detected in frequency during the 4-AP treatment (Fig. 5*E*). Concomitantly, a significant decrease (0.64 ± 0.09-fold decrease when compared with baseline) was detected in the 3xTg-AD group during and after 4-AP stimulation (Fig. 5*F*). Once again, no notable change was detected in the frequency of theta activity during and after 4-AP treatment in the 3xTg-AD group (Fig. 5*G*). Overall, the young 3xTg-AD mice were characterized by a less excitable hippocampal network activity.

Discussion

In this study, we assessed the structural and functional changes to pyramidal neurons from 3xTg-AD mice at the very early stage of disease progression (P30). Interestingly, we found that most of the pyramidal neurons in the CA1–3, in subiculum regions, and in some PARV+ hippocampal interneurons from the 1-month-old 3xTg-AD group increased the levels of phosphorylated Tau protein at MDr sites (Fig. 1 and 2).

Because pyramidal cells and PARV+ interneurons are mainly responsible for the generation and maintenance of theta rhythms (18), our data suggested the existence of very early changes in hippocampal oscillatory activity that could affect cognitive function. Importantly, it has been proposed that low-frequency neural entrainment in the neural theta bands provides a mechanism to represent and integrate temporal information (29–31).

To isolate the correlation of hyperphosphorylated Tau protein in hippocampal circuit activity, we recorded the spontaneously generated theta activity in the pyramidal cell layer of the 3xTg-AD model. Our data revealed that spontaneously generated theta oscillations are altered as early as 30 days of age in the 3xTg-AD group (Fig. 3). Specifically, we found a significant reduction in rhythmicity and a significant increase in theta frequency (Fig. 3). Further supporting our findings, pyramidal cells from 3xTg-AD mice had significant power increase of subthreshold membrane oscillations and reduction of the spike accommodation (Fig. 3 and Table 1).

Similarly, changes in hippocampal theta activity have been correlated with the cognitive deficit observed during neurodegeneration (32). Specifically, slowing of hippocampal activity has been correlated with cognitive decline in early onset AD (33). Considering this, the increase in theta frequency in our study argues against the decline of hippocampal-dependent behavioral tasks. Aiming to explore this possibility, we performed the nesting and burrowing tests in the young 3xTg-AD model. Accordingly, our 1-month-old 3xTg-AD group did not show hippocampal-dependent behavioral abnormalities (Fig. 4). In the 3xTg-AD model, alterations in hippocampal-dependent tasks are detected as early as 4 months of age (34), hence supporting our findings. Altogether, our work provides evidence that the electrophysiological changes precede memory impairment in the 3xTg-AD model. Thus, our data postulate very early alterations in theta activity as a potential biomarker that precedes any detected cognitive deficit observed during neurodegeneration. To further support our conclusions, the hypothesis that alterations in network activity, specifically hypersynchronous network activity preceding protein deposition and cognitive dysfunction in AD models, has been widely recognized (35–37).

Although there was no evidence of cognitive deficit in the P30 3xTg-AD model, abnormal excitability in the CA3 hippocampal network was recently reported (38). To study the level of the hippocampal circuit excitability in the CA1/subiculum pyramidal cell layer of the young 3xTg-AD model, we bath-applied 4-AP while recording theta activity (Fig. 5). Blocking of Kv potassium channels with 4-AP, in TgCRND8 at early P30, increased theta power and induced seizure activity (22). Altogether, our data demonstrated for the first time that the CA1 hippocampal network in the TgCRND8 AD mouse model showed hyperexcitability preceding protein deposition and cognitive impairments (22). However, the blocking of Kv channels in the P30 3xTg-AD mouse model exerted the opposite effect; the CA1/subiculum hippocampal network showed sig-

Figure 3. Young 3xTg-AD mice were characterized by alterations in theta activity. *A*, representative traces of network oscillatory activity recorded in the CA1/subiculum area of non-Tg mice. *B*, theta band activity magnification of sample window from non-Tg mice. *C*, filtered traces at theta band frequency (3–8 Hz) from non-Tg mice. *D*, representative traces from theta activity recorded at CA1/subiculum of 3xTg-AD mice. *E*, theta band activity magnification of sample window from 3xTg-AD mice. *F*, filtered traces at theta band frequency (3–8 Hz) from 3xTg-AD mice. *G* and *H*, spectrograms (400 s) from the same recordings shown above (*G* and *H*, respectively). *I*, statistical analysis of theta oscillation strength confirmed lower values in the 3xTg-AD group when compared with the non-Tg group. *J*, statistics showed the increase in average oscillation frequency from the 3xTg-AD group when compared with the non-Tg group. *K*, micrograph and recording position in the septo-hippocampal preparation. *L*, comparison of subthreshold membrane oscillations and spike accommodation in 3xTg-AD and non-Tg group. *M*, graphic representation of subthreshold membrane oscillations in the 3xTg-AD group when compared with the non-Tg group. *N*, graphic representation of spike accommodation in the 3xTg-AD group when compared with the non-Tg group. All *bar graphs* show means ± S.E. *, $p < 0.05$.

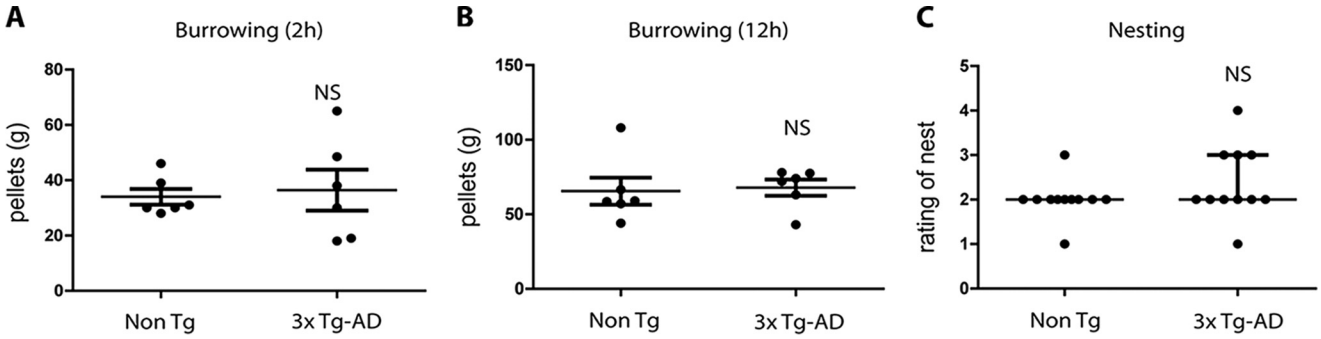

Figure 4. 3xTg-AD mice did not show behavioral abnormalities at 30 days of age. 3xTg-AD and non-Tg mice were analyzed in the burrowing (*A* and *B*) and nesting tests (*C*) at 30 days of age. No significant differences were observed in either test between non-Tg and 3xTg-AD groups (*A–C*). All *bar graphs* show means ± S.E. *NS*, $p \geq 0.05$).

nificantly reduced excitability when compared with the non-Tg group (Fig. 5). In addition, seizure susceptibility in young 3xTg-AD mice was significantly diminished (Fig. 5). Of relevance, whole-cell 4-AP–sensitive K^+ current amplitude did not change from 1 to 6 months of age and was not different in 3xTg-AD mice compared with in WT in CA1, CA3, or dentate neurons (19).

Altogether, these findings suggest the activation of homeostatic mechanisms that aim to protect the hippocampal network excitability levels. As previously mentioned, we reported that Tau phosphorylation at MDr sites could serve as a regulatory mechanism to prevent overexcitation (11). Specifically, we reported that increases in sites Thr^{231}, Ser^{235}, Ser^{396}, and Ser^{404} reduced susceptibility to excitotoxicity by perturbing the PSD-95–Tau–Fyn synaptic complex, therefore promoting the synaptic response to depression rather than to potentiation (11). Recently, it has been reported that increased Tau phosphorylation inhibits β-amyloid toxicity and prevents seizure activity in AD transgenic mice, thus supporting our hypothesis (13).

Importantly, our results do not rule out the possibility that the accumulated increase of hyperphosphorylated Tau exerts deleterious effect on neural system function at later stages in the disease. However, our data showed that although the increase in phosphorylated Tau at very early stages has no effect on hippocampal-dependent tasks, it could protect the hippocampal circuit from overexcitation.

Overall, our findings demonstrated that induced seizure activity decreases in young 3xTg-AD mice and an increase in Tau phosphorylation at MDr sites could mitigate hyperexcitability by directly interacting with the pyramidal circuitry that spontaneously generates theta oscillations. These findings are in line with our previous findings where we proposed that Tau phosphorylation at MDr sites could serve as a regulatory mechanism that prevents NMDA receptor overexcitation produced by Aβ (11). Also, the data presented in this document are also important because they contradicted the current and leading hypothesis that postulates Tau protein phosphorylation as mainly a pathological response. Instead, the data presented in this document, along with our previous data (3, 11), showed that Tau phosphorylation at the initial stages of disease progression could represent a compensatory mechanism that mediates neuroprotection against hyperexcitability. Finally, further studies on AD and other tauopathies are needed to fully understand the biological roles and post-translational modifications of Tau protein (12).

Experimental procedures

Animals

Male 30–35-day-old 3xTg-AD and age-matched nontransgenic (non-Tg) mice from strain B6129SF2/J (The Jackson Laboratory) were housed in groups of 2–4 animals and maintained on a 12:12 light cycle with water and food available *ad libitum*. Experimental procedures were approved by the Bioethics committee of the Institute of Neurobiology, UNAM. Genotype was confirmed by PCR (The Jackson Laboratory protocol). The mice were taken from their home cage and sacrificed by decapitation.

Electrophysiology

3xTg-AD and non-Tg mice (aged 30–35 days) were decapitated, and the brain was rapidly removed and placed in ice-cold high sucrose artificial cerebrospinal fluid (ACSF) solution (252 mM sucrose, 3 mM KCl, 2 mM $MgSO_4$ 24 mM $NaHCO_3$, 1.25 mM NaH_2PO_4, 1.2 mM $CaCl_2$, and 10 mM glucose) and bubbled with carbogen (95% O_2 and 5% CO_2). A glass plate (inverted Petri dish) covered with lens paper was used as the stage for most of the dissection. The glass plate can be rotated on the crushed ice throughout the dissection to gain access to various parts of the hippocampus with the dissection instruments. The cerebellum and frontal cortex were removed with a razor blade, and the hemispheres were separated and allowed to recover for 2–3 min in the oxygenated sucrose solution. Complete septo-hippocampal isolate was then removed from the remaining hemisection as described previously (17). In sum, one spatula supported the inner portion of the cortical hemisphere, and the other was used to gently pull away the brainstem and thalamus to expose the hippocampal artery and underlying CA3 and dentate gyrus. To separate the hippocampus from the cortex, the spatula was again placed between the cortex and extreme dorsal end of the hippocampus and moved smoothly through to the caudal portion of cortex. During this process the spatula helped separate the CA1/subicular tissue from the overlying cortex. The hippocampal complex was removed from the surrounding brain tissue by placing one spatula on the CA3/dentate gyrus region of the dorsal hippocampus and pulling the dorsal hippocampus toward to the caudal portion of the brain. Blood

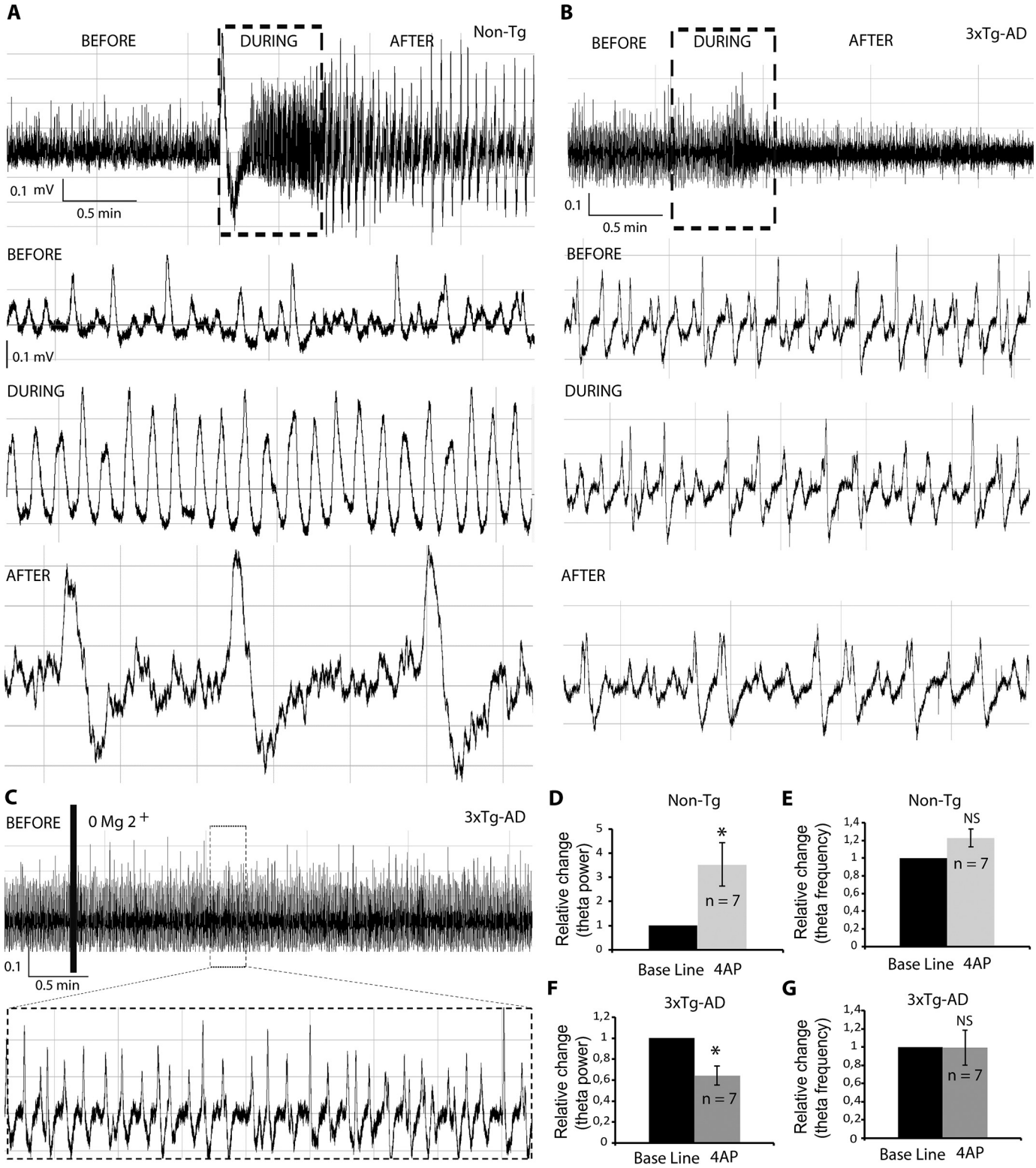

Figure 5. 3xTg-AD mice were characterized by a less excitable hippocampal network. *A* and *B*, raw traces of theta oscillations recorded in the CA1/subiculum area of non-Tg (*A*) and 3xTg-AD mice (*B*). In the non-Tg group, 4-AP increased theta amplitude during (*A*, *black rectangle* and *lower panel*) and after stimulation (*A*, *lower panel*). In the 3xTg-AD group, 4-AP decreased theta amplitude during (*B*, *black rectangle* and *lower panel*) and after stimulation (*B*, *lower panel*). *C*, zero Mg^{2+} did not elicit detectable changes in the amplitude and frequency of theta activity in the 3xTg-AD mice. *D*, the theta power increase for non-Tg animals under 4-AP stimulation was statistically confirmed. *E*, no significant changes were observed in theta frequency for the non-Tg group when treated with 4-AP. *F*, a statistically significant decrease in theta amplitude was found in the 4-AP 3xTg-AD treated group. *G*, no significant changes in frequency were detected in the 4-AP 3xTg-AD group. All *bar graphs* show means ± S.E. *, $p < 0.05$; *NS*, $p \geq 0.05$.

vessels may impede prompt removal and should be cut away but not ripped out to avoid unnecessary tissue damage. The entire hippocampal isolation procedure was completed within 1 min. Any remaining cortex was removed using micro-scissors when the preparation was returned to the oxygenated sucrose solution. After dissection, the complete septo-hippocampal preparation was left at room temperature in ACSF bubbled with carbogen for 60 min. For recording, the preparation was transferred quickly to a custom-made submerged recording chamber. Recordings were performed at 30–32 °C after an additional 30-min period in the chamber. The preparation was continuously perfused with ACSF (25 ml/min, 126 mM NaCl, 24 mM $NaHCO_3$, 10 mM glucose, 4.5 mM KCl, 2 mM $MgSO_4$, 1.25 mM NaH_2PO_4, and 2 mM $CaCl_2$, pH 7.4, with 95% O_2/5% CO_2) via a gravity-fed perfusion system and maintained at 30–32 °C. Local field potentials were recorded using glass micropipettes (2–6 MΩ) filled with ACSF. The signals were recorded through a differential AC amplifier (A-M Systems), filtered online (0.1–500 Hz), and sampled at 5 KHz. The wave shape of the theta oscillation varied according to frequency and maintained a symmetrical near-sinusoidal shape like *in vivo* theta rhythm. This hippocampal theta was observed using normal artificial cerebrospinal fluid. Power spectra were calculated using the multitaper method (Chronux toolbox) using seven tapers. Integrated theta-band power was calculated in 5-s bins over a period of 2–14 min, and the mean spectrum was taken as the grand mean of each animal. Changes in theta power were measured in mV^2/Hz.

All drugs came from aliquots of stock solutions (stored at −80 °C) and were added to the perfusing artificial ACSF at the concentrations indicated. Base line recording lasted for 20 min followed by 0.5 min of pharmacological stimulation (4-AP at 150 μM) and 20 min recovery after stimulation.

Patch recordings

The animals were anesthetized with sodium pentobarbital (63 mg/kg) and perfused transcardially with cold modified artificial cerebrospinal fluid with the following composition: 238 mM sucrose, 3 mM KCl, 2.5 mM $MgCl_2$, 2 mM $NaHCO_3$, and 30 mM D-glucose, pH 7.4, and bubbled with carbogen (95% O_2 and 5% CO_2). After a maximum of 1.5 min of transcardial perfusion, the animals were decapitated, and the brains were removed and dissected in ice-cold ACSF containing the following: 119 mM NaCl, 3 mM KCl, 1.5 mM $CaCl_2$, 2 mM $MgCl_2$, 25 mM $NaHCO_3$, and 30 mM D-glucose, pH 7.4. One cerebral hemisphere was mounted onto an agar block with a 30 grades inclination. Slices (400 μm thick) containing the hippocampal formation were cut with a vibratome (Thermo Scientific HM650V). The slices were left to recover at room temperature for at least 60 min before experimental manipulation. Whole-cell patch–clamp recordings were obtained using the visual patch–clamp technique with an Axo-clamp 2B amplifier (Axon Instruments, Foster City, CA). The cells were aimed for and recorded based on their location CA1 pyramidal layer of the hippocampus. Neurons from non-Tg and 3xTg-AD mice were recorded. Patch electrodes (4–8 MΩ) were pulled from filamented borosilicate glass tubes (G150F-4; Warner Instruments, Handem, CT) and filled with a solution containing: 140 mM potassium gluconic acid, 10 mM EGTA, 2 mM $MgCl_2$, 10 mM HEPES, 2 mM Na_2ATP, and 2 mM LiGTP, pH 7.4. Cell characterization was performed by injecting 0–600-pA, 600-ms-long depolarizing and hyperpolarizing current steps. Recordings were restricted to neurons located within the CA1/subiculum portion of the hippocampus. Whole-cell recordings were kept for analysis only if the neuron remained stationary throughout the recording, spikes overshot 0 mV, and access resistance was <30 MΩ.

Hippocampal dependent behavioral task

For nesting, 1 h before the dark phase each mouse ($n = 12$) was transferred to an individual cage wood-chip bedding but without environmental enrichment items. We placed a cotton square (5 × 5 cm) on each cage. The following morning the nests were assessed, according to Deacon (23–27) as follows: 1) Nestlet not noticeably touched (>90% intact). 2) Nestlet partially torn up (50–90% remaining intact). 3) Mostly shredded but often no identifiable nest site: <50% of the nestlet remains intact but <90% is within a quarter of the cage floor area, *i.e.* the cotton is not gathered into a nest but spread around the cage. Note: the material may sometimes be in a broadly defined nest area, but the critical definition is that 50–90% has been shredded. 4) An identifiable, but flat nest: >90% of the nestlet is torn up, the material is gathered into a nest within a quarter of the cage floor area, but the nest is flat, with walls higher than mouse body height (curled up on its side) on less than 50% of its circumference. 5) A near perfect nest: >90% of the nestlet is torn up, and the nest is a crater, with walls higher than mouse body height on more than 50% of its circumference.

For burrowing, a day before the test, the cage mates were moved as two separated groups from their home cage to a larger rat cage (26 × 48 × 20 cm). We placed burrow consisting of a plastic black tube, 20 cm long and 7.5 cm in diameter, which was raised 2.5 cm by two screws bolted at the open end. The lower end of a burrow was closed off, and the tube contained 200 g of standard mouse food pellets. We let both groups do the task during the night to improve burrowing ability and diminish variability between animals. In the next session, 3 h before the dark phase of the cycle, the mice were placed individually in rat cages containing a burrow filled with 200 g of food pellets; the animals had access to water, but there was not extra food to keep them focused on the task. The amount of food pellets displaced after the first 2 h of the test was recorded. The burrow was refilled, and the test continued overnight and the following morning. The weight of the pellets removed from the burrow was recorded.

Immunohistochemistry

Additional male mice were anesthetized by pentobarbital and transcardially perfused (PBS followed by 4% paraformaldehyde). The brains were stored in fixative for 24 h at 4 °C and then in a sucrose solution (30% in PBS) for 3 days at 4 °C; frozen using dimethylbutane; and stored at −80 °C. The brains were sliced coronally using a freezing microtome at 40 μm for light microscopy or using a vibrating microtome at 50 μm for fluorescence microscopy, and free-floating sections were stored in a preservative solution (3:3:4 glycerol:ethylene glycol:PBS) at −20 °C in preparation for immunohistochemistry staining.

The serial sectioning fraction for immunohistochemistry was ⅛). Washes in PBS preceded all steps except primary antibody addition. All steps were at room temperature unless otherwise specified.

For immunofluorescence, the sections were incubated for 2 h with PBS containing 1% normal goat serum, 0.25% Triton X-100, and 0.45% gelatin. The sections were further incubated overnight at 4 °C with phospho-Tau (Ser^{396}), AT180, and anti-PARV–positive (Thermo Fisher and Sigma–Aldrich). The sections were incubated for 2 h with secondary antibody (Alexa 488–596–conjugated goat anti-rabbit; 1:2000 dilution). The sections were then mounted on glass slides with Vectashield mounting medium (Vectorlabs). Fluorescence was visualized using an epifluorescence (Axioplan2; Zeiss) microscope. The CA1/subiculum/CA3 areas were observed with 20× objective. High magnification photomicrograph was obtained with a 40× objective.

Western blotting

For Western blotting analysis, total protein from hippocampal preparations were obtained by lysis buffer. A total of 15–20 μg of total protein was loaded on a 10% SDS-PAGE, separated and transferred onto Immobilon-P transfer membranes (Millipore). The following antibodies and dilutions were used: Tau5 (mAb against total Tau, Abcam, 1:2000. Tau5 antibody detects all six Tau isoforms and depending on gel migration different band sizes could be detected) and phospho-Tau (Ser^{396}) (mAb against phosphorylated Tau, Thermo Fisher, 1:2000). To evaluate differences in Tau phosphorylation, equal amounts of total protein from 3xTg-AD and non-Tg animals were loaded. The blots were developed using ECL-Plus (GE Healthcare) or Supersignal West Femto (Pierce). The results were quantified with ImageJ software and were normalized to the total Tau protein signal.

Data analysis

Using custom MATLAB software, field traces were filtered and analyzed using a Fourier transform. Autocorrelogram of the filtered theta signal was used to derive a value reflecting the degree of rhythmicity. All data were analyzed statistically by either, pairwise comparisons with Student's *t* tests or Mann–Whitney *U* test using STATISTICA 7 (StatSoft, Inc.). In all tests, values of $p < 0.05$ were considered to indicate significance. *Bar graphs* show experimental means, with *error bars* indicating standard error of the mean.

Author contributions—S. M.-R. conceptualization; S. M.-R., F. P.-O., S. D.-C., G. P., and S. W. resources; S. M.-R. data curation; S. M.-R. software; S. M.-R., A. S.-G., and B. O. formal analysis; S. M.-R. supervision; S. M.-R. funding acquisition; S. M.-R. validation; S. M.-R., A. S.-G., M. M., B. O., and E. O.-S. investigation; S. M.-R. visualization; S. M.-R., M. M., E. O.-S., and S. W. methodology; S. M.-R. writing-original draft; S. M.-R. project administration.

Acknowledgments—We thank Jessica Gonzalez Norris for proofreading, Kevin Yiron Frias Arroyo for comments on the manuscript, and Dr. Elvira Galarraga Palacio for the use of anti-PARV+ antibody.

References

1. Gouw, A. A., Alsema, A. M., Tijms, B. M., Borta, A., Scheltens, P., Stam, C. J., and van der Flier, W. M. (2017) EEG spectral analysis as a putative early prognostic biomarker in nondemented, amyloid positive subjects. *Neurobiol. Aging* **57,** 133–142 CrossRef Medline
2. Lei, M., Xu, H., Li, Z., Wang, Z., O'Malley, T. T., Zhang, D., Walsh, D. M., Xu, P., Selkoe, D. J., and Li, S. (2016) Soluble Aβ oligomers impair hippocampal LTP by disrupting glutamatergic/GABAergic balance. *Neurobiol Dis.* **85,** 111–121 CrossRef Medline
3. Mondragón-Rodríguez, S., Perry, G., Luna-Muñoz, J., Acevedo-Aquino, M. C., and Williams, S. (2014) Phosphorylation of Tau protein at sites $Ser^{396-404}$ is one of the earliest events in Alzheimer's disease and Down syndrome. *Neuropathol. Appl. Neurobiol.* **40,** 121–135 CrossRef Medline
4. LaFerla, F. M., Green, K. N., and Oddo, S. (2007) Intracellular amyloid-β in Alzheimer's disease. *Nat. Rev. Neurosci.* **8,** 499–509 CrossRef Medline
5. Kaniyappan, S., Chandupatla, R. R., Mandelkow, E.-M., and Mandelkow, E. (2017) Extracellular low-n oligomers of Tau cause selective synaptotoxicity without affecting cell viability. *Alzheimer's Dement.* **13,** 1270–1291 Medline
6. Chishti, M. A., Yang, D.-S., Janus, C., Phinney, A. L., Horne, P., Pearson, J., Strome, R., Zuker, N., Loukides, J., French, J., Turner, S., Lozza, G., Grilli, M., Kunicki, S., Morissette, C., *et al.* (2001) Early-onset amyloid deposition and cognitive deficits in transgenic mice expressing a double mutant form of amyloid precursor protein 695. *J. Biol. Chem.* **276,** 21562–21570 CrossRef Medline
7. Mucke, L., and Selkoe, D. J. (2012) Neurotoxicity of amyloid-protein: synaptic and network dysfunction. *Cold Spring Harb. Perspect. Med.* **2,** a006338 Medline
8. Salgado-Puga, K., Rodríguez-Colorado, J., Prado-Alcalá, R. A., and Peña-Ortega, F. (2017) Subclinical doses of ATP-sensitive potassium channel modulators prevent alterations in memory and synaptic plasticity induced by amyloid-β. *J. Alzheimer's Dis.* **57,** 205–226 Medline
9. Ittner, L. M., Ke, Y. D., Delerue, F., Bi, M., Gladbach, A., van Eersel, J., Wölfing, H., Chieng, B. C., Christie, M. J., Napier, I. A., Eckert, A., Staufenbiel, M., Hardeman, E., and Götz, J. (2010) Dendritic function of Tau mediates amyloid-β toxicity in Alzheimer's disease mouse models. *Cell* **142,** 387–397 CrossRef Medline
10. Goedert, M. (1999) Alzheimer's disease: Pinning down phosphorylated Tau. *Nature* **399,** 739–740 CrossRef Medline
11. Mondragón-Rodríguez, S., Trillaud-Doppia, E., Dudilot, A., Bourgeois, C., Lauzon, M., Leclerc, N., and Boehm, J. (2012) Interaction of endogenous Tau with synaptic proteins is regulated by NMDA-receptor dependent Tau phosphorylation. *J. Biol. Chem.* **287,** 32040–32053 CrossRef Medline
12. Mondragón-Rodríguez, S., Perry, G., Zhu, X., and Boehm, J. (2012) Amyloid β and Tau proteins as therapeutic targets for Alzheimer's disease treatment: rethinking the current strategy. *Int. J. Alzheimers Dis.* **2012,** 630182 Medline
13. Ittner, A., Chua, S. W., Bertz, J., Volkerling, A., van der Hoven, J., Gladbach, A., Przybyla, M., Bi, M., van Hummel, A., Stevens, C. H., Ippati, S., Suh, L. S., Macmillan, A., Sutherland, G., Kril, J. J., *et al.* (2016) Site-specific phosphorylation of Tau inhibits amyloid-β toxicity in Alzheimer's mice. *Science* **354,** 904–908 CrossRef Medline
14. Soler, H., Dorca-Arévalo, J., González, M., Rubio, S. E., Ávila, J., Soriano, E., and Pascual, M. (2017) The GABAergic septohippocampal connection is impaired in a mouse model of tauopathy. *Neurobiol. Aging* **49,** 40–51 CrossRef Medline
15. Oddo, S., Caccamo, A., Shepherd, J. D., Murphy, M. P., Golde, T. E., Kayed, R., Metherate, R., Mattson, M. P., Akbari, Y., and LaFerla, F. M. (2003) Triple-transgenic model of Alzheimer's disease with plaques and tangles: intracellular Aβ and synaptic dysfunction. *Neuron* **39,** 409–421 CrossRef Medline
16. Buzsáki, G., Anastassiou, C. A., and Koch, C. (2012) The origin of extracellular fields and currents: EEG, ECoG, LFP and spikes. *Nat. Rev. Neurosci.* **13,** 407–420 CrossRef Medline
17. Goutagny, R., Jackson, J., and Williams, S. (2009) Self-generated theta oscillations in the hippocampus. *Nat. Neurosci.* **12,** 1491–1493 CrossRef Medline

18. Bénédicte Amilhon, B., Huh, C. Y., Dé, F., Manseau, F., Ducharme, G., Nichol, H., Adamantidis, A., and Williams, S. (2015) Parvalbumin interneurons of hippocampus tune population activity at theta frequency. *Neuron* **86,** 1277–1289 CrossRef Medline
19. Wang, Y., and Mattson, M. P. (2014) L-type Ca^{2+} currents at CA1 synapses, but not CA3 or dentate granule neuron synapses, are increased in 3xTgAD mice in an age-dependent manner. *Neurobiol. Aging* **35,** 88–95 CrossRef Medline
20. García Méndez, K. M., Macías, M., González Pereyra, P., Salas Gallardo, A., Williams, S., Peña Ortega, F., and Mondragón-Rodríguez, S. (2017) Characterizing the hippocampal theta's response to carbachol; using a complete septo-hippocampal preparation. *Ing. Biomed.* **38,** 208–215 CrossRef
21. Goutagny, R., Gu, N., Cavanagh, C., Jackson, J., Chabot, J. G., Quirion, R., Krantic, S., and Williams, S. (2013) Alterations in hippocampal network oscillations and theta-gamma coupling arise before Aβ overproduction in a mouse model of Alzheimer's disease. *Eur. J. Neurosci.* **37,** 1896–1902 CrossRef Medline
22. Mahar, I., Albuquerque, M. S., Mondragon-Rodriguez, S., Cavanagh, C., Davoli, M. A., Chabot, J. G., Williams, S., Mechawar, N., Quirion, R., and Krantic, S. (2016) Phenotypic alterations in hippocampal NPY- and PV-expressing interneurons in a presymptomatic transgenic mouse model of Alzheimer's disease. *Front. Aging Neurosci.* **8,** 327 Medline
23. Deacon, R. M., Raley, J. M., Perry, V. H., and Rawlins, J. N. (2001) Burrowing into prion disease. *Neuroreport* **12,** 2053–2057 CrossRef Medline
24. Deacon, R. (2012) Assessing burrowing, nest construction, and hoarding in mice. *J. Vis. Exp.* e2607s CrossRef Medline
25. Deacon, R. M., Croucher, A., and Rawlins, J. N. (2002) Hippocampal cytotoxic lesion effects on species-typical behaviours in mice. *Behav. Brain Res.* **132,** 203–213 CrossRef Medline
26. Deacon, R. M., Penny, C., and Rawlins, J. N. (2003) Effects of medial prefrontal cortex cytotoxic lesions in mice. *Behav. Brain Res.* **139,** 139–155 CrossRef Medline
27. Deacon, R. M. (2006) Burrowing in rodents: a sensitive method for detecting behavioral dysfunction. *Nat. Protoc.* **1,** 118–121 CrossRef Medline
28. Shiri, Z., Lévesque, M., Etter, G., Manseau, F., Williams, S., and Avoli, M. (2017) Optogenetic low-frequency stimulation of specific neuronal populations abates ictogenesis. *J. Neurosci.* **37,** 2999–3008 CrossRef Medline
29. Colgin, L. L. (2016) Rhythms of the hippocampal network. *Nat. Rev. Neurosci.* **17,** 239–249 CrossRef Medline
30. Hasselmo, M. E., and Brandon, M. P. (2012) A model combining oscillations and attractor dynamics for generation of grid cell firing. *Front. Neural Circuits* **6,** 30 Medline
31. Patel, J., Fujisawa, S., Berényi, A., Royer, S., and Buzsáki, G. (2012) Traveling theta waves along the entire septotemporal axis of the hippocampus. *Neuron* **75,** 410–417 CrossRef Medline
32. Cayzac, S., Mons, N., Ginguay, A., Allinquant, B., Jeantet, Y., and Cho, Y. H. (2015) Altered hippocampal information coding and network synchrony in APP-PS1 mice. *Neurobiol. Aging* **36,** 3200–3213 CrossRef Medline
33. Engels, M. M., Hillebrand, A., van der Flier, W. M., Stam, C. J., Scheltens, P., and van Straaten, E. C. (2016) Slowing of hippocampal activity correlates with cognitive decline in early onset Alzheimer's disease: an MEG study with virtual electrodes. *Front. Hum. Neurosci.* **10,** 238 Medline
34. Oddo, S., Caccamo, A., Kitazawa, M., Tseng, B. P., and LaFerla, F. M. (2003) Amyloid deposition precedes tangle formation in a triple transgenic model of Alzheimer's disease. *Neurobiol. Aging* **24,** 1063–1070 CrossRef Medline
35. Palop, J. J., and Mucke, L. (2016) Network abnormalities and interneuron dysfunction in Alzheimer disease. *Nat. Rev. Neurosci.* **17,** 777–792 CrossRef Medline
36. Verret, L., Mann, E. O., Hang, G. B., Barth, A. M., Cobos, I., Ho, K., Devidze, N., Masliah, E., Kreitzer, A. C., Mody, I., Mucke, L., and Palop, J. J. (2012) Inhibitory interneuron deficit links altered network activity and cognitive dysfunction in Alzheimer model. *Cell* **149,** 708–721 CrossRef Medline
37. Mondragón-Rodríguez, S., Perry, G., Peña-Ortega, F., and Williams, S. (2017) Tau, amyloid β and deep brain stimulation: aiming to restore cognitive deficit in Alzheimer's disease. *Curr. Alzheimer Res.* **14,** 40–46 CrossRef Medline
38. Kazim, S. F., Chuang, S.-C., Zhao, W., Wong, R. K., Bianchi, R., and Iqbal, K. (2017) Early-onset network hyperexcitability in presymptomatic Alzheimer's disease transgenic mice is suppressed by passive immunization with anti-human APP/Aβ antibody and by mGluR5 blockade. *Front. Aging Neurosci.* **9,** 71 Medline